Channeling of low-energy ions on hydrogen-covered single-crystal surfaces

Robert D. Kolasinski,[1,*] Norman C. Bartelt,[2] Josh A. Whaley,[1] and Thomas E. Felter[1]
[1]*Sandia National Laboratories, Hydrogen and Metallurgical Science Department, Livermore, California 94551, USA*
[2]*Sandia National Laboratories, Materials Physics Department, Livermore, California 94551, USA*
(Received 5 August 2011; revised manuscript received 25 January 2012; published 19 March 2012)

Low-energy ion beam techniques such as direct recoil spectroscopy (DRS) are well-suited for directly detecting adsorbed hydrogen. However, with this approach it has previously only been possible to detect the hydrogen configuration on single-crystal surfaces for a narrow range of conditions (e.g., when the adsorbate atoms reside close to the surface). In this study we investigate the experimental and modeling tools needed to extend DRS to a much wider range of adsorption geometries. At grazing incidence, we show how adsorbed hydrogen affects ion focusing along open surface channels, thereby revealing fine details about the binding geometry even for adsorbates residing high above the substrate. Under such conditions, the scattering process is characterized by ions interacting with many atoms simultaneously. Therefore interpreting these types of measurements properly requires realistic molecular dynamics (MD) simulations with accurate scattering potentials at large distances. As an illustration of the progress that can be made, we consider how hydrogen is recoiled from W(100)+H(ads) during exposure to a low-energy (1 keV) Ne^+ analysis beam at grazing incidence. The closest approach distance of the ions is >1 Å, making hydrogen located high above the substrate readily accessible. By mapping the hydrogen recoils over different crystallographic directions using DRS, we identify focusing mechanisms that provide information on the adsorbed hydrogen configuration. When W(100) is continuously dosed with H_2(g) to maintain a saturation coverage, we observe enhanced recoil signals along the ⟨100⟩ and ⟨110⟩ azimuths consistent with hydrogen residing in bridge sites. The reproduction of the complex experimental scattering spectra by our MD modeling techniques offers a pathway to locate hydrogen well within its vibrational envelope.

DOI: 10.1103/PhysRevB.85.115422 PACS number(s): 68.43.−h, 34.50.−s, 61.85.+p, 68.49.Sf

I. INTRODUCTION

Hydrogen-metal interactions have received considerable attention, particularly because of their relevance to hydrides,[1] hydrogen energy infrastructure,[2] and plasma-facing components in magnetic fusion reactors.[3] However, determining the detailed configuration of adsorbed hydrogen can be a notoriously difficult task. Limited understanding of H chemisorption sites has been inferred from electron-based techniques[4–6] and more recently from scanning tunneling microscopy (STM).[7] However, the hydrogen atoms themselves only subtly affect the detected signal, and positive identification of the binding configuration is problematic. In such situations, changes in the substrate from reconstruction can easily overwhelm any observable effect from the adsorbate. Thus, the extensive literature on surface reconstructions altered by H adsorption relies on indirect measurements to infer the hydrogen binding sites.

It has been known for quite some time that low-energy ion beam techniques are capable of detecting hydrogen and other light adsorbates directly.[8–11] Low-energy ion scattering (LEIS) and direct recoil spectroscopy (DRS) are two closely related diagnostics especially well-suited for this purpose, since they provide both surface compositional and structural information. Despite the advantage of direct sensitivity to hydrogen, hydrogen binding sites have been determined only in specialized cases with these techniques. Multiple collisions often contribute to the detected ion signals, which complicate the analysis. This has undoubtedly hindered efforts to analyze hydrogen binding, and any improvements to the experiments or their interpretation would be particularly welcome.

At this point, it is worth pointing out that the difference between the two techniques (as their respective names suggest) is whether the detected species are scattered incident ions (LEIS) or recoils from the substrate/adsorbate (DRS). While different collision processes contribute to the detected ion signals, in general the same analyzer collects both species during the measurement. In both cases, the detected particle energies provide information on the surface composition, whereas shadowing and focusing effects between adjacent atoms provide information on the local atomic structure. A key concept used for structural analysis is the "shadow cone," which is a region of space behind a surface atom that incident ions cannot reach. Surface atoms that are shadowed do not contribute to the detected signal. Conversely, atoms just outside of a shadow cone receive a higher flux due to focusing. If the interatomic potential between the incident ions and surface atoms is well known, the shadow cone dimensions can be calculated in a straightforward manner using a variety of analytical expressions.[12,13] This enables atomic positions to be determined in real space. It is important to keep in mind that adsorbed hydrogen does not strongly deflect even light ions (He^+, Li^+, and Ne^+) typically used to probe the surface. To determine the location of the hydrogen, the incident particles can be focused by substrate atoms. These conditions make DRS the natural choice for detecting hydrogen, although LEIS has also been successfully used in several cases.[8] Given the strong nature of shadowing and focusing, the detected hydrogen recoil signal then can be expected to depend critically on the adatom location relative to the substrate atoms.

A. Prior approaches to detecting hydrogen with low-energy ion beams

It is worth considering under what conditions it has been previously possible to determine the hydrogen configuration successfully. Past studies suggest that when it resides close to the surface (such as in hollow sites or in the troughs between atom rows), the hydrogen can be readily detected using DRS and analyzed using conventional shadow cone analysis. However, density functional theory (DFT) predictions indicate that it is not uncommon for hydrogen to reside at heights of 1 Å or more.[14] Assuming a typical shadow cone shape, grazing angles of incidence would be needed to focus the ions into the adsorbate atoms. Under such conditions, the ions interact with an extended region of the surface, and the binary collision approximation (BCA) fails. This renders many of the simpler tools commonly used to model ion scattering (e.g., MARLOWE[15]) inaccurate.

Improvements to low-energy ion beam techniques for hydrogen detection could be realized by using an analysis beam angled at grazing incidence. In such situations the energy of the ions perpendicular to their direction of flight is very small. This increases the distance of closest approach to the outermost atoms, providing access to hydrogen located high above the surface. One approach would be to characterize the angular distribution of forward scattered ions with a large solid-angle microchannel plate detector, using a procedure similar to that of Schüller and coworkers to analyze the Fe(110)+O and Fe(110)+S systems.[16] In principle, the presence of hydrogen might be inferred by their effect on the trajectories of scattered ions, thereby providing a possible pathway for detection. In the present study we detect recoiled hydrogen directly using DRS. In this configuration (illustrated in Fig. 1), ions directed at grazing incidence angles are gently steered by the heavy substrate atoms and then undergo hard (small impact parameter) collisions with the hydrogen atoms. These hydrogen atoms are recoiled at large angles and can be readily detected using a conventional electrostatic analyzer or time of flight system. To extract useful information from the recoil signals, the paths of the incident ions traveling along surface channels and the hydrogen ejected from the surface must be well understood.

B. The W(100)+H(ads) model system

To test our modeling and experimental approaches, we consider the W(100)+H model system. W(100) is ideally suited for grazing incidence measurements, particularly because tungsten is a high-Z material and can deflect incoming ions even at large distances from the surface. Early LEED measurements show a $c(2 \times 2)$-H phase on W(100) for low hydrogen coverage at 25 °C,[17] later attributed to reconstruction.[4,5] The surface reverts to a (1×1) configuration once the coverage approaches saturation. Subsequent measurements with STM[18] have since confirmed these findings.

For the (1×1) phase at saturation hydrogen coverage, off-specular HREELS[6,19] and inelastic He scattering measurements[20] provide evidence of hydrogen binding to bridge (twofold) sites through vibrational analysis. Infrared vibrational spectra also support these findings.[21] The saturation coverage (2×10^{15} H/cm^2) estimated from ion beam analysis[22] and work function measurements[4] are also consistent with bridge site occupation (2 H/W). Prior DFT calculations for unreconstructed W(100) largely are in accord with the experimental findings, showing the energy for adsorption at bridge sites is 0.4 eV lower than at fourfold hollow sites and 0.7 eV more favorable than at top sites.[14,23]

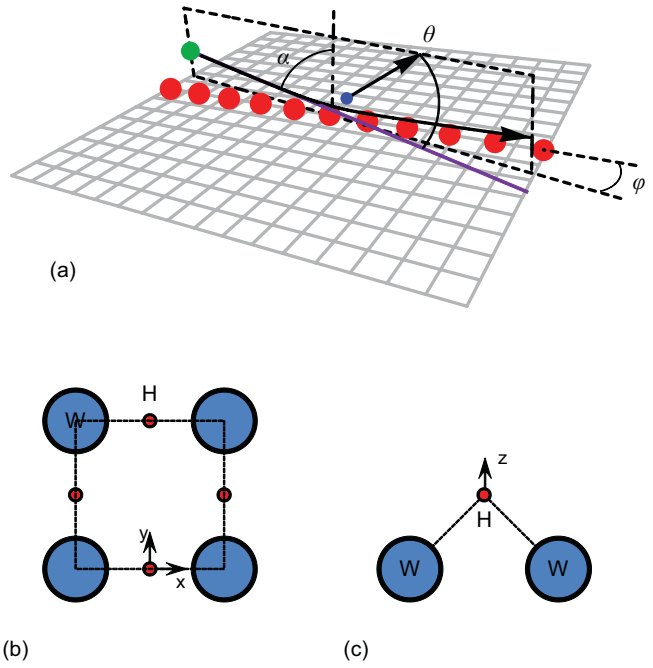

FIG. 1. (Color online) (a) Scattering geometry for an ion deflected by a single row of surface atoms at grazing incidence. A single recoil atom produced by a hard collision is also shown, along with the definitions for the incidence (α), azimuth (φ), and observation (θ) angles. The vibrational model proposed by Barnes and Willis (Ref. 19) for H residing within bridge sites on W(100) are shown from both top (b) and side (c) perspectives.

Binding to the partially covered $c(2 \times 2)$-H surface has been less extensively studied. Based upon HREELS measurements, Barnes and Willis[19] developed a vibrational model for H that fits bridge site binding of H on W(100) at all coverages. In Fig. 1 we provide an illustration of the three vibrational modes from their proposed model. The remaining two vibrational modes are parallel and perpendicular to the plane containing the W-H-W bond, as shown in case (b). Case (c) illustrates a stretch mode perpendicular to the surface. Barnes and Willis considered coverage factions ranging between 0.01 and 1.0 (saturation) and found that the HREELS energy-loss peaks shifted with coverage. They attributed the shift to changes in the W-H-W bond angle resulting from the effect of reconstruction on the lateral spacing of surface W. It was concluded that hydrogen preferentially binds to "short" bridge sites in the reconstructed surface at partial coverage.

C. Experimental and modeling approach

The objective of this work is to demonstrate the feasibility of using the DRS approach previously outlined for detecting H adsorbed on surfaces. For this purpose we consider the well-characterized adsorption system W(100)+H(ads). Based on a combination of previously published experimental results

and our own theoretical calculations, we are able to use this surface as a model for scattering measurements. Using an angle resolved ion energy spectrometer (ARIES) we mapped hydrogen recoil signals along different surface channels using DRS. With a simple qualitative model of surface channeling, we are able to show how these recoil intensity patterns are uniquely related to the positioning of the hydrogen atoms on the surface. We then apply molecular dynamics (MD) simulations to accurately model the scattering and measure the adsorbate height.

II. MODELING HYDROGEN ADSORPTION ON W(100) WITH DFT

The prior experimental and modeling work on W(100)+H(ads) suggests a well-defined picture of how W(100) behaves with a saturation coverage of hydrogen. However, a detailed comparison of the different binding sites at low coverage has not been studied extensively. To clarify the understanding for intermediate coverage on the reconstructed surface, we performed our own first-principles calculations using the DFT code VASP (Vienna *ab initio* simulation package).[24] To compute the binding geometry of H on W(100), we used the Perdew-Burke-Ernzerhof (PBE) implementation of the generalized gradient approximation[25] and the projector-augmented wave approximation.[26,27] We modeled the W(100) substrate as a four-layer slab, with hydrogen adsorbed on top of it. The positions of the atoms of the lower layer were fixed at their theoretical bulk W locations (a_{PBE} 3.16 Å); all other atom positions were relaxed until forces on them were <0.03 eV/Å in magnitude. For accuracy, we used a 700 eV plane-wave basis cutoff and sampled the 2×2 surface brillouin zone with an 8×8 set of equally spaced k-vectors. We accelerated electronic relaxation through Methfessel-Paxton Fermi level smearing[28] (width $= 0.2$ eV).

As a preliminary measure, we calculated the binding configuration for the saturation coverage case, i.e., (1×1) W(100)+H. We found the bridge site to be much more energetically favorable than the fourfold hollow site, a result that is in accord with previous work by White *et al.*[14] Our predictions of the adsorbate height above the first plane of substrate atoms (given in Table I) also compare well with this prior work. As expected, when we simulated a partial coverage of hydrogen ($\Theta = 1$), the first-layer tungsten atoms displaced into a $c(2 \times 2)$-H configuration. The substrate atom displacements from DFT were in reasonable agreement with the experimental findings of Barnes and Willis,[19] who measured $\delta \geqslant 0.30 \pm 0.05$ Å. In this configuration our DFT calculations predict that H resides in the short bridge sites at a height of 1.42 Å above the surface, or about 0.32 Å higher than in the saturated (1×1) configuration. All sites examined near the fourfold hollow location were found to be unstable.

TABLE I. Hydrogen configuration on W(100) predicted by DFT.

Fourfold hollow	$h = 0.49$ Å	$\Theta_{\mathrm{H}} = 1$ H/W
Bridge	$h = 1.10$ Å	$\Theta_{\mathrm{H}} = 2$ H/W
Reconstructed bridge	$h = 1.42$ Å	$\Theta_{\mathrm{H}} = 1$ H/W
Tungsten displacement	$\delta = 0.31$ Å	$\Theta_{\mathrm{H}} = 1$ H/W

TABLE II. DFT predictions of RMS vibrational amplitudes of H on W(100).

$\sqrt{\langle x^2 \rangle} = 0.057$ Å
$\sqrt{\langle y^2 \rangle} = 0.12$ Å
$\sqrt{\langle z^2 \rangle} = 0.078$ Å

The positioning of the adsorbed hydrogen atoms will also be affected by thermal vibrations and could potentially affect any experimentally observed scattering signals. With the model proposed by Barnes and Willis in mind,[19] we calculated the response of the adsorbed hydrogen to small displacements using DFT along the three axes referenced in Fig. 1. The calculated RMS vibrational amplitudes at room temperature are listed in Table II. The most striking characteristic of these results is the large amplitude along the y axis (perpendicular to the plane containing the W-H-W bond) in comparison to the other axes. A likely explanation is that along this direction the adsorbed H has very little interaction with the neighboring atoms that would counteract small displacements. We found this effect to be even stronger at lower coverage where fewer hydrogen atoms are in neighboring sites.

III. EXPERIMENTAL CONFIGURATION AND SAMPLE PREPARATION

We performed LEIS and DRS measurements using an angle-resolved ion energy spectrometer (ARIES) configured specifically for studies of light adsorbates. Further details regarding the instrument and our experimental procedures may be found in our prior work.[29,30] For the experiments discussed herein, the mass-separated incident beam consists of 1 keV Ne^+ ions rastered over a 2×2 mm area, with current densities between 4.0×10^{12} and 1.5×10^{13} cm^{-2} s^{-1}. An electrostatic energy analyzer collects forward scattered and recoiled particles and can be positioned at angles ranging between $20^\circ \leqslant \theta \leqslant 90^\circ$. [Scattering angles are illustrated in Fig. 1(a).] For most of the measurements presented in this article, we used a detection angle of $\theta = 45^\circ$. The spectrometer is mounted on a rotatable stage with the 2 mm diameter circular acceptance aperture located 18.5 mm away from the sample. We measured the energy spread of the beam by passing it directly through the analyzer; at 3 keV the full width at half maximum was approximately 1 eV.

The surface of our single crystal (MaTecK) was oriented within 0.1° of the (100) crystal plane. To prevent undesired masking effects at grazing incidence, we secured the crystal about its periphery by a Ta wire. Our precision manipulator allows the angle between the polished surface and the incident beam to be determined to within 0.1°. A heater mounted behind the sample enables temperatures up to 1200 °C to be maintained, and impurities were removed by cycles of sputter cleaning and annealing. Adding hydrogen to tungsten surfaces is straightforward since there is no barrier to dissociative chemisorption; simply introducing H_2(g) at partial pressures above 10^{-7} torr saturates the surface. The base pressure in our vacuum system was 4×10^{-10} torr, with H_2(g) comprising most of the residual gas species.

An important consideration for the scattering and recoil maps is the possibility for ion-induced damage to degrade the surface structure. Upon initial consideration, one might expect damage to the W(100) substrate to deteriorate the W(s) signal variation with azimuth. However, we noted no such difference between measurements taken before and after mapping. One possible explanation is that the low sputtering yield and high damage threshold for W exposed to low-energy Ne^+ ions mitigates some of the dose-dependent effects of the ion beam. Taking into account that defects in W become mobile and begin to anneal at temperatures above 400 °C,[31] we used periodic heating cycles to further ameliorate damage and to help reorder the surface. During the measurements, the incident beam also recoils hydrogen from the surface, thereby creating vacancies within the adsorbate layer. However, this was quickly replenished by continuous exposure of the sample surface to hydrogen.

IV. DRS MEASUREMENTS

An experimental ion energy spectrum obtained at room temperature is shown in Fig. 2 for 1 keV $Ne^+ \rightarrow W(100)$. The scattering geometry, including the angle of incidence (α), the scattering angle (θ), and the azimuth (φ) are also indicated. Note that the $\varphi = 0^\circ$ azimuth aligns with the $\langle 100 \rangle$ direction, as shown in the inset. Even in the absence of H_2 dosing (as is the case for this spectrum), a small peak associated with recoiling H atoms still persists, due to residual H_2 within the system. For $\theta = 45^\circ$, a peak associated with the single elastic recoil H occurs at $E/E_0 = 0.090$. The locations of scattering (s) and recoil (r) peaks associated with O and W are also noted in Fig. 2. One striking feature of the spectrum is the peak at $E/E_0 = 0.14$, above the H single elastic recoil energy. This behavior was also observed in prior work by Bastasz,[32,33] who found the most plausible explanation was multiple surface scattering/recoil events involving hydrogen. At more grazing incidence, this secondary peak disappears. The signal intensity centered at $E/E_0 = 0.75$ did not correspond to any expected impurities within our system. Moreover, the height of this peak varied with temperature in a strikingly similar manner to the H(r) signal. To provide further insight into the origin of this intensity we used a modified version of the binary collision code MARLOWE,[15] which provided specialized output detailing the incident ion and recoiling atom trajectories. These simulations reproduce this intensity structure and indicate it originates from Ne^+ atoms which lose energy by interacting with the adsorbed H layer prior to detection.

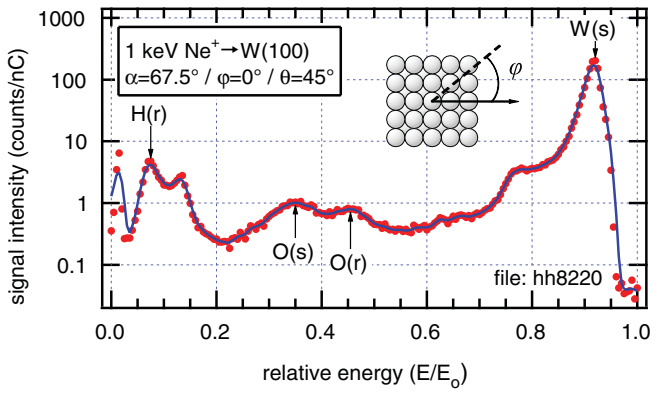

FIG. 2. (Color online) Ion energy spectrum for 1 keV $Ne^+ \rightarrow W(100)$, obtained at room temperature. Peaks due to scattered Ne^+ are marked with the notation (s); recoils are indicated with the notation (r). Inset: Top view of the W(100) surface showing reference direction for $\varphi = 0^\circ$.

Oxygen impurities on the tungsten surface can potentially affect hydrogen adsorption. To estimate the coverage of these impurities, we calculated the respective cross-sections for 1 keV Ne^+ ions scattering from W and O using the Biersack-Haggmark approximation for the scattering integrals and the Ziegler-Biersack-Littmark potential and screening. Integrating the W(s) and O(s) peaks in Fig. 2 and scaling them according to their respective cross-sections, we estimate the surface coverage to be 1.8%. A similar estimate can be performed for the O(r) peak, yielding a coverage of 0.7%. This is likely an underestimate given the low ionization fraction for the recoiling oxygen. Nevertheless, these estimates suggest that the oxygen concentration is safely below 2%.

The substrate configuration will certainly influence where hydrogen binds to the surface, making a preliminary check of local atomic structure particularly worthwhile. A series of azimuthal scans performed at discrete polar angles quickly revealed the fourfold symmetry of the W(100) surface. Using shadow cone analysis, we found that the scattering signals indicated that the W atoms reside in locations close to their bulk-terminated locations.

Having characterized the surface composition and verified the substrate structure, analyzing the hydrogen recoil signals is now possible. For this purpose we constructed hydrogen recoil maps which show the variation of the H(r) signal over a wide range of α and φ. We probe the surface with 1 keV Ne^+ and monitor the relative energy $E/E_0 = 0.090$ associated with the single elastic recoil peak for H. We considered polar angles ranging between $70.53 \leqslant \alpha \leqslant 84.26$ over a complete 360° rotation in azimuth (φ). The maps shown in Fig. 3 have been rendered from a grid of 29 × 181 angular positions using first-order interpolation but are otherwise unaltered from the raw data (i.e., no reflection has been performed).

For the recoil maps depicted in Fig. 3, the coloration indicates recoil intensity in counts/nC, and key crystallographic directions are provided on the top axis. Case (a) depicts the H(r) intensity when the surface has been dosed with H_2(g) at a pressure of 10^{-6} torr at 25 °C to reach saturation coverage. Recall that under these circumstances we expect the W(100) surface to be in a (1 × 1) phase with H atoms residing in bridge sites. Case (b) corresponds to partial hydrogen coverage (from the residual amount remaining in the vacuum system) where the substrate is expected to have reconstructed to a $c(2 \times 2)$ configuration. Finally in case (c), we have heated the crystal to 300 °C to desorb all but a small concentration of H on the surface. For all three maps the energy of the incident Ne^+ ion beam was 1 keV. Note that $\varphi = 0^\circ$ has been referenced to the $\langle 100 \rangle$ set of azimuths along the surface, and a detector angle of $\theta = 45^\circ$ was used.

In Fig. 3(a) the fourfold symmetry of the recoil intensity pattern is instantly recognizable with two different structures visible. For $\alpha < 75^\circ$, the H(r) peaks occur along the $\langle 100 \rangle$ azimuths. In the range $78^\circ \leqslant \alpha \leqslant 83^\circ$, a secondary set of

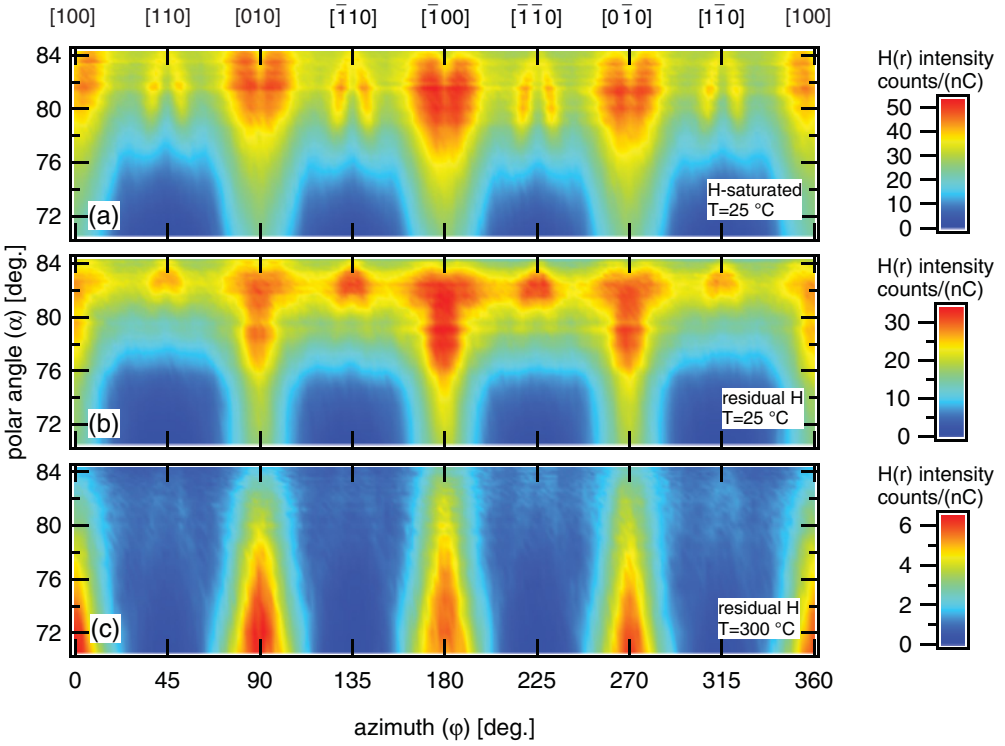

FIG. 3. (Color) Recoil intensity maps from the W(100) surface exposed to (a) a H_2(g) pressure of 10^{-6} torr with $T_{surf} = 25\,^{\circ}$C; (b) residual H_2(g) with $T_{surf} = 25\,^{\circ}$C; and (c) residual H_2(g) with $T_{surf} = 300\,^{\circ}$C. The maps were obtained with a 1 keV Ne^+ analysis beam.

maxima paired along the ⟨110⟩ directions emerges, gradually converging as α increases. The residual hydrogen case depicted in Fig. 3(b) displays qualitatively similar characteristics to case (a), although the intensity patterns along the ⟨110⟩ azimuths are less distinct by comparison whereas the structure centered along the ⟨100⟩ directions is narrower. For minimal hydrogen coverage at elevated temperature shown in Fig. 3(c), the hydrogen signal is completely different from the previous two cases. Here, the recoil signal is only visible along the ⟨100⟩ azimuths and becomes more intense at lower α.

V. INTERPRETATION OF THE RECOIL MAPS

The maps presented in Fig. 3 provide clear evidence of ion-focusing effects that, if properly interpreted, could reveal the adsorbate configuration. The problem then becomes how to extract this information from the experimental data. For the (1×1) phase at saturation coverage, three high symmetry sites (top, bridge, and hollow) are illustrated in Fig. 4, along with the first layer tungsten atoms. As previously discussed, the regions of highest recoil intensity in Fig. 3(a) (corresponding to saturation coverage at room temperature) are centered along the ⟨100⟩ and ⟨110⟩ azimuths. Incident ions are deflected away from W atom rows, and any configuration where the hydrogen resides within the open directions (channels) would increase the recoil yield. The shaded regions in Fig. 4 illustrate the prominent channels and the three high symmetry-binding conditions. Only when the bridge sites are occupied does an unobstructed row of H atoms reside along both the ⟨100⟩ and ⟨110⟩ channeling directions (highlighted by the dashed line). Therefore, bridge site bonding is more consistent with our experimental measurements at saturation coverage, a finding that is in accord with previously published work and our DFT model.

The similarities between the maps depicted in Figs. 3(a) and 3(b) suggest that the preferred binding configuration remains similar even at lower coverage. Some subtle differences exist and could be due to substrate reconstruction or changes in ion focusing as the hydrogen coverage is decreased. Recall that when the W(100) surface reconstructs to form a $c(2 \times 2)$ phase at partial coverage, the first-layer tungsten atoms are displaced 0.31 Å laterally from their positions in the (1×1) configuration. This modifies the channel geometry along the ⟨100⟩ directions. In addition, less hydrogen is available in the surface channels to deflect ions.

The high temperature/low coverage map in Fig. 3(c) shows a much different behavior. The patterns along the ⟨110⟩

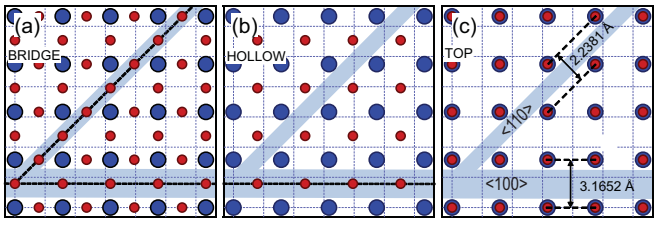

FIG. 4. (Color) Possible hydrogen binding configurations for the W(100) surface with prominent channeling directions indicated by the shaded regions. When bridge sites are occupied, unobstructed rows of hydrogen atoms lie within channels along both the ⟨100⟩ and ⟨110⟩ directions, as illustrated by the dashed lines in case (a). First-layer W atoms are represented by blue markers, whereas adsorbed H are indicated in red.

directions are now nearly absent, and the recoil signals along the ⟨100⟩ azimuths are most intense at steeper incidence angles. We were able to eliminate any possibility of significant changes in the substrate structure using LEIS, based upon azimuthal scans that revealed a fourfold symmetry identical to our measurements at higher coverage. Based on this, we must conclude that the hydrogen binding configuration is different for our high temperature/low coverage case. The intensity structure visible at lower angles of incidence is consistent with binding deep within the ⟨100⟩ surface channels.

VI. SIMULATING SCATTERING AND RECOIL PROCESSES USING MD

While much insight can be gained from the simple analysis presented in the previous section, clearly some of the more subtle effects identified cannot be addressed without more detailed models of surface channeling. When selecting the most appropriate modeling approach, it is important to keep in mind that the recoil maps presented in Sec. IV include signals recorded at grazing incidence, making the projectile energy perpendicular to the surface (defined here as $E_\perp = E_0\cos^2(\alpha)$, where E_0 is the incident energy) very small. The most grazing incidence angle included in the maps was $\alpha = 84.26^\circ$, where the perpendicular energy is a very modest $E_\perp = 10$ eV for $E_0 = 1$ keV. Many surface atoms influence the ion trajectories simultaneously under these conditions, thereby invalidating the BCA commonly incorporated into sputtering and scattering. Furthermore, because shadow cone dimensions are calculated based upon the BCA, their use here is also questionable. This clearly indicates that a more sophisticated MD approach is needed.

A good summary of the theoretical aspects of grazing incidence scattering can be found in previous work by Winter[34] and Danailov.[35,36] To calculate focusing along the ⟨100⟩ and ⟨110⟩ directions, we use the Kalypso[37] MD package (version 3.1). We begin by initializing ion trajectories 3 Å above the surface where the influence of the substrate atoms is minimal. The area of the surface that the incident particles interact with dictates the size of the simulation domain and depends on α; for the most grazing incidence angle used in our experiments, we found a 40 Å length to be sufficient. The computational time can be reduced considerably by taking advantage of the shadowing of second layer of W atoms for $\alpha > 76^\circ$. To account for neutralization, we employed a straightforward approach outlined by Rabalais *et al.*[38] This model suggests the impact parameter of the collision and the path of the recoiled particle away from the surface are the two main factors that affect the fraction of recoils which emerge from the surface as ions. While this approach is relatively simple, it enabled us to reproduce the experimental results in a satisfactory manner.

In the MD simulations we take into account random thermal displacements of first-layer tungsten atoms, which occur far more slowly than the ion flight time (therefore appearing to be immobilized during the simulation timescale). These displacements tend to smear out some of the focusing that would otherwise occur on a perfect single crystal near 0 K.[35] Here we assumed that the first-layer atoms had a Debye temperature that was smaller than the bulk by a factor of 0.71, based on values tabulated by Waldfried *et al.*[39] The bulk Debye temperature, based on x-ray scattering, was 310.21 K. In addition, we also considered two possible cases for the vibrational amplitudes of the adsorbed hydrogen. In our initial calculations we estimated the Debye temperature of the hydrogen to be approximately 1000 K. We later refined this model using the DFT results described in Sec. II. Surprisingly our initial estimate, which assumed larger vibrational amplitudes, provided qualitatively a better approximation to our experimental results. A likely explanation is that step edges and other crystal imperfections are also present on the surface and would disrupt the ion focusing in a manner similar to increasing the vibrational amplitude of the adsorbed hydrogen. For a more rigorous fitting of the experimental data, one could incorporate these effects into a more detailed MD model of the surface.

A fundamental question is: how much do the incident ions interact with the hydrogen layer at grazing incidence? The distance of closest approach to the surface, $z_{\min}$, can be roughly estimated by considering where the interatomic potential (V_i) is strong enough to counteract the transverse energy of the incident particle ($E_\perp$).[34–36] (Details on how the interatomic potential is calculated will be provided in a later section.) Whereas the corrugations in the potential transverse to the beam tend to focus the particle trajectories azimuthally, the incident ions are not particularly sensitive to variations parallel to the direction of flight. Hence, it is possible to use a "string" calculation[40] to approximate the potential due to a row of atoms:

$$V_s(\rho) = \frac{1}{d}\int_{-\infty}^{\infty} V\{[x^2+\rho^2]^{1/2}\}dx.$$

In the expression above, d is the interatomic spacing along the atom row, whereas ρ represents perpendicular distance from the atom row. In Fig. 5 we plot equipotential contours

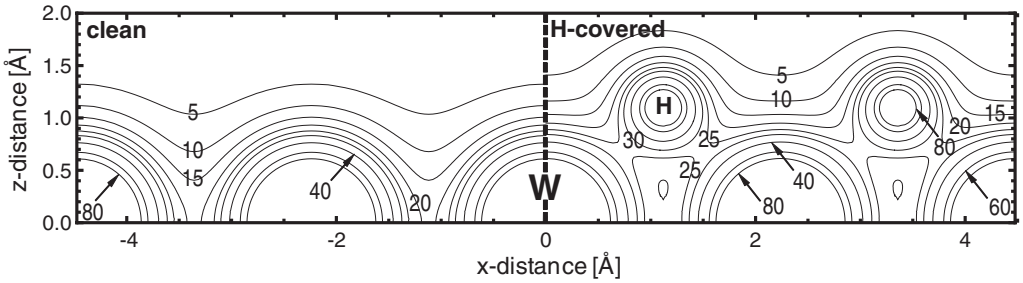

FIG. 5. Potential contours for Ne→W(100) along the ⟨110⟩ direction. The contours for the clean surface are depicted on the left, whereas the right-hand side shows the potential when hydrogen resides in bridge sites. Labels indicate the potential strength in eV.

for Ne→W(100)+H, summing the contributions of W and H atoms along the ⟨110⟩ direction. The left-hand side of the plot shows the contours for a clean surface, whereas the right-hand side shows the potential for a H-saturated surface. Note that even at distances of 1 Å above the surface, $V_i > 10$ eV. This verifies that the incident ions will interact with the surface hydrogen over a long portion of their trajectories.

For a given surface channel configuration, the ion trajectories will be most strongly influenced by two factors: the adsorbate height and the potentials for both the Ne-H and Ne-W interactions. For the scattering calculations discussed here, the energies involved in the collisions are sufficiently high that only the repulsive portion of the potential needs to be considered. While the universal interatomic potential developed by Ziegler, Biersack, and Littmark (ZBL)[41] is satisfactory for most applications, it is worth considering recent work by Scüller *et al.*[16] and Winter *et al.*,[42] who developed a very elegant and precise approach for measuring the interatomic potentials based on rainbow scattering of low-energy atoms. Their measurements reveal for many different systems that individual pair potentials (calculated with isolated-atom electron distributions) much more accurately reproduce the scattering behavior along surface channels than the ZBL potential. One possible explanation is that the ZBL potential is an average of many individual pair-potentials and therefore neglects the details of specific interactions. In addition, the solid-state Hartree-Fock electron distributions incorporated in the ZBL fit are more appropriate for modeling collisions in the lattice during sputtering and ion implantation calculations rather than for grazing incidence scattering. Strikingly, for every system they considered, the ZBL fit predicted a stronger interaction at large impact parameters than did the isolated atom calculation. A similar result was found by Karolewski, who compared DFT calculations with the ZBL fit for a number of projectile-target combinations.[43]

Unfortunately, measurements of the Ne-W potential have not been yet made using the precise approach of Schüller and Winter. Nevertheless, the existing experimental database for other systems motivated us to model the interaction using more rigorous computational approaches. Here we determine the Ne-H potential using both a direct integration procedure developed by Wedepohl[44] and DFT calculations. The basic analytical approach involves calculating the electrostatic forces between the two atoms as their electron shells overlap, as well as kinetic and exchange effects. We determined the radial electron distributions using Slater-type orbitals from Ref. 45 and neglected any distortion of the electron shells during the interaction. The DFT simulations were carried out once again using VASP. The Ne-W and Ne-H interactions were computed in the same way as described in Sec. II, except that the two atoms were positioned at various separations in a $10 \times 10 \times 10$ Å box with periodic boundary conditions. Figures 6(a) and 6(b) compares the calculated results with the ZBL fit for Ne-H and Ne-W potentials, respectively. At small interatomic separations, the agreement between all three approaches is satisfactory; however, at larger distances both the DFT and analytical calculations predict a substantially weaker interaction between the Ne and H. The agreement between the pair potential calculation and the DFT results remains good for interaction energies as low as 1 eV, where they begin to diverge.

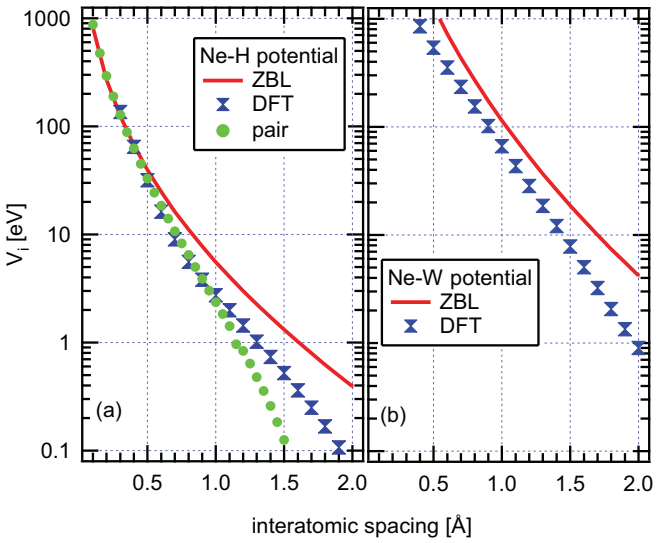

FIG. 6. (Color online) Calculated (a) Ne→H and (b) Ne→W interatomic potentials.

Nevertheless, the agreement is excellent for $V_i > 10$ eV, which is of sufficient accuracy for the aims of this study. The Ne-W potential is similarly predicted to be much more repulsive by the ZBL potential when compared with DFT, as illustrated in Fig. 6(b). This result mirrors the general findings of the previously discussed work of Schüller *et al.*,[16] Winter *et al.*,[42] and Karolewski.[43]

VII. COMPARISON BETWEEN SIMULATIONS AND EXPERIMENT: SATURATION COVERAGE CASE

Using Kaylpso, we simulated Ne^+ ion impingement along the ⟨100⟩ and ⟨110⟩ surface channels and recorded the energies of the recoiled hydrogen atoms assuming different adsorbate configurations. Rather than undertake the time-consuming process of simulating an entire recoil map, we instead consider a small subset of scattering/recoil geometries. This makes it easier to observe the effect of systematically adjusting parameters such as the adsorbate height and the interatomic potential. To make the calculations as efficient as possible, it is common practice to minimize the number of atoms included in the simulation domain, in many cases including only atoms along a particular surface channel. Such an approach is feasible if one is only interested in trajectories that are perfectly parallel with channel, whereas here scattering events along different crystal azimuths are also of interest. To balance this need with the desire for computation efficiency, we assembled separate models for the ⟨100⟩ and ⟨110⟩ channels, which included additional rows of atoms on either side. Using this approach, we were able to simulate recoil signals within ±14° of the ⟨100⟩ azimuth and ±12° of the ⟨110⟩ direction, covering the most important portions of the azimuthal scans at representative polar angles. The experimental azimuthal scan shown in Fig. 7(a) corresponds to the horizontal "cut" in the saturation coverage recoil map in Fig. 3(a) at $\alpha = 81.5°$. By calculating the recoil behavior for different adsorbate configurations and comparing with experiment, one can identify the correct configuration. For this

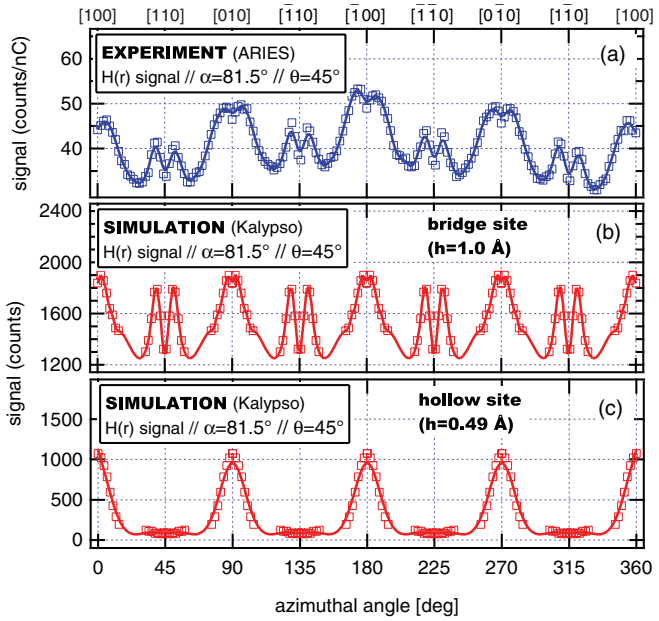

FIG. 7. (Color online) Azimuthal variation of the hydrogen recoil intensity for a polar angle of $\alpha = 81.5°$ obtained for a saturated surface. Case (a) depicts the experimental data for these conditions, whereas case (b) illustrates a corresponding Kalypso simulation assuming bridge site occupation ($h = 1.0$ Å). Case (c) shows the expected intensity variation assuming the hollow sites are filled, with the adsorbate height selected to correspond to our DFT calculations ($h = 0.49$ Å). For reference, we indicate the major azimuths on the surface along top axis. The solid line is a spline fit intended to guide the eye between the individual simulations (indicated by the markers).

purpose we considered both the fourfold hollow and bridge configurations, incorporating adsorbate heights predicted by DFT. The simulated hydrogen recoil patterns for both of these cases are illustrated in Figs. 7(b) and 7(c).

The recoil signals produced assuming hydrogen occupies bridge sites are depicted in Fig. 7(b) and largely replicate the features of the experimental data: the twin peaks about the ⟨110⟩ azimuths and a larger peak at the ⟨100⟩ azimuths. (The role of adsorbate height is discussed below.) Conversely, the hollow site data shown in panel (c) fails to capture any of the recoil intensity along the ⟨110⟩ directions.

This highlights one of the important advantages of DRS insofar as different surface binding sites for the hydrogen will result in completely different recoil intensity patterns. Our simulations support the assertion that hydrogen occupies bridge sites at saturation coverage, a finding that is consistent both with our DFT calculations and prior experimental results. These findings also validate the channeling mechanisms proposed at the beginning of Sec. V. An assumed height of 1.0 Å above the first-layer tungsten plane provides qualitative agreement with experiment.

More detailed information about the intensity patterns portrayed in the maps can be understood by considering the ion trajectories themselves. For example, perfect alignment between the ion beam and either of the surface channels causes a dip in the recoil intensity. Understanding this effect is relatively straightforward, as illustrated by the trajectories along the ⟨110⟩ channel depicted in Fig. 8. Here we have incorporated the bridge site geometry predicted by the DFT calculations and verified by our experiments, with each panel on the left showing a "top view," i.e., a plane containing the first-layer tungsten atoms. For clarity, thermal vibrations have been eliminated and the horizontal scale has been compressed to emphasize deflections along the channel axis. The panels to the right depict a view along the channel axis.

Figure 8(a) shows trajectories for a clean surface, where the tungsten surface atoms tend to focus the Ne^+ ions toward the center of the ⟨110⟩ channel. The addition of a single hydrogen atom within the channel would not be expected to significantly alter the ion trajectories. However, adding an entire row of hydrogen results in the scenario depicted in Fig. 8(b). Although there is no well-defined shadow cone for Ne→H, the hydrogen effectively deflects the neon ions away from the centerline. This shadowing effect disappears with a slight rotation in azimuth away from perfect alignment. This phenomenon is responsible for the recoil signal variation along the ⟨110⟩ directions and to some extent also along the ⟨100⟩ azimuths. One would expect this effect to be sensitive to several factors, including the adsorbate height, its concentration on the surface, the interatomic potential, as well as the scattering geometry (α and φ). Assuming the last three parameters are fixed or accurately known, then the adsorbate height can be measured. While there are no direct measurements of the Ne-W and Ne-H scattering potentials for the energies of interest here, the calculation techniques we adopted here have accurately reproduced the observed rainbow scattering patterns for many ion-target combinations.[16,42]

Consider Fig. 8(c), which depicts ion trajectories for the same conditions as case (b) except for the potential. Here we used the ZBL prediction for the Ne→H interaction, rather than our fit to the DFT simulations. The ion trajectories are surprisingly sensitive to this adjustment: since the ZBL potential is more repulsive than our DFT potential, the ions are deflected by much larger angles by the row of hydrogen. For grazing incidence simulations, this emphasizes the need for accurate potential calculations at low energies. Note also that decreasing the concentration of hydrogen on the surface would naturally diminish the strength of the shadowing effect. This is discussed in greater detail in the following section.

Figure 9 illustrates how varying the adsorbate height in the bridge site affects the observed recoil patterns. Four different heights are shown in cases (a) through (d). (Height refers to the distance above the first-layer plane of tungsten.) When the hydrogen resides relatively close to the surface ($h = 0.8$ Å), the azimuthal variation of the H(r) signal is relatively unremarkable. Recoil signals are enhanced along open channels where hydrogen resides, as one would expect based on the qualitative analysis presented in Sec. V. However, as the height is increased, the hydrogen contributes more strongly to the ion focusing, and the shadowing effects discussed in the previous paragraphs become more important. As can be seen in case (b) for $h = 1.0$ Å, this sharply diminishes the recoil intensity when the ion beam is precisely aligned with the ⟨110⟩ azimuths. This effect is still evident, although less dramatic, along the ⟨100⟩ channels. Nevertheless, as the height of the hydrogen is increased, the shadowing becomes much more pronounced, as illustrated in cases (c) and (d). From a

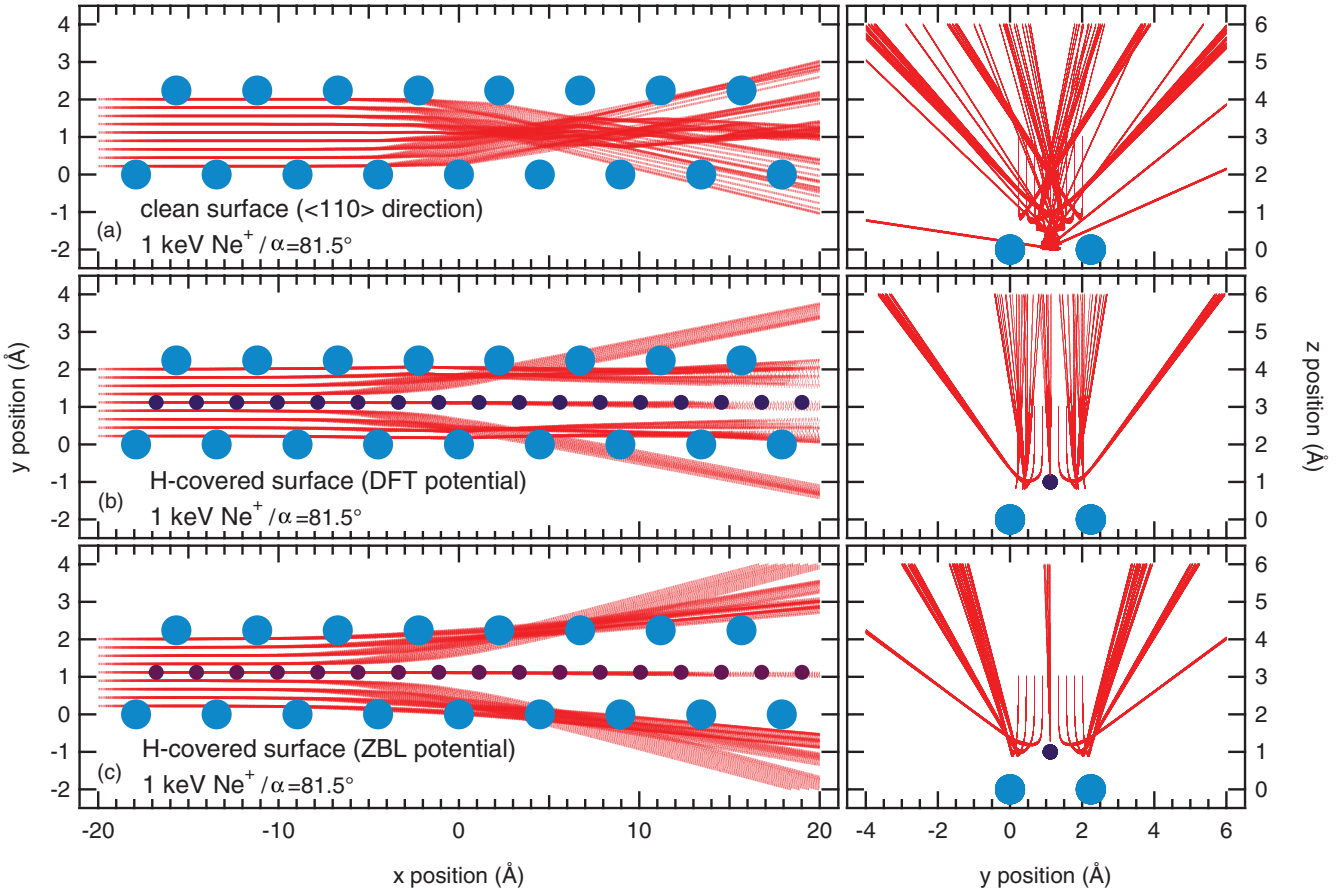

FIG. 8. (Color) Ion trajectories calculated using molecular dynamics for 1 keV Ne^+ scattering along the ⟨110⟩ azimuth within the W(100) surface. The different panels depict scattering for (a) a clean surface, (b) a hydrogen-covered surface using our DFT potential to model the Ne→H interaction, and (c) a hydrogen-covered surface using the ZBL potential for the Ne→H interaction. In both (b) and (c) we have assumed hydrogen occupies bridge sites at $h = 1.0$ Å. Each panel contains both a top view on the left and end view on the right, with coordinate axes clarifying the different vantage points. Large circular markers indicate the tungsten substrate; the smaller markers indicate adsorbed hydrogen.

qualitative perspective, an adsorbate height close to the DFT predictions ($h = 1.0$ Å) provides the best comparison with the experimental results.

Using straightforward binary collision models, we have shown in our prior work[30,46] the benefits of using quantitative comparisons between simulated and experimental ion scattering maps to determine the configuration of atoms on surfaces. Using reliability factors (R-factors), one can find the best fit to a variety of simulated configurations in an unbiased manner. This is the logical next step in applying the techniques outlined here to more rigorously make comparisons between simulations and experiments. These results bring up the question of what further effects must be taken into consideration to rigorously quantify the height of the hydrogen atoms above the surface. As discussed in the previous section, a more accurate accounting for the effect of thermal vibrations and surface imperfections (e.g., step edges) would be needed for this purpose. We would expect these to contribute less strongly to the observed recoil signals than the interatomic potential and particularly the binding site. Their main effect would be to blur some of the focusing effects described previously.

Simulating an entire series of maps using MD for a quantitative comparison between the experiments and models would require further development. The W(100)+H(ads) surface, at saturation coverage, is composed of simple open channels that gently steer the ions and efficiently shadow deeper tungsten atoms. Under these circumstances a simplified substrate that includes only atoms along these surface channels suffices, and a usable surface model can be as small as 100 atoms. A disadvantage to this approach is that it limits us to considering conditions where the incident ions were aligned to within $\pm 14^\circ$ of the channel. (Larger misalignments would cause the incident ions to escape to another part of the surface.) With these simplifications, each test case depicted in Fig. 9 required ∼1 week to execute on a single processor. For the more complex structures possible arising from surface reconstruction, the geometry is not as favorable. In addition, step edges and other surface imperfections are present in the experimental system, and their effect must be accounted for in our models. At this level of complexity (when the simulation domain includes thousands of atoms), more advanced computing approaches becomes a necessity. Nevertheless, we do not foresee any insurmountable obstacles

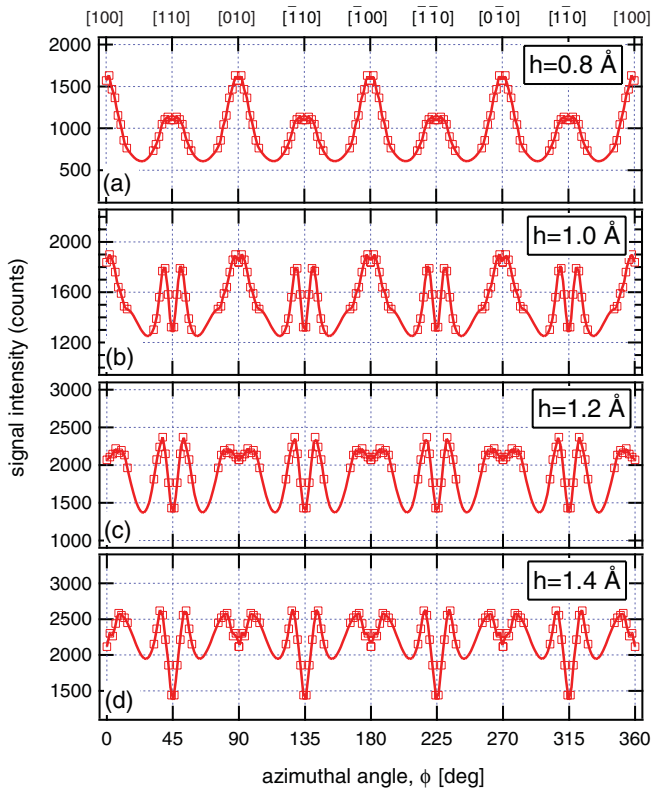

FIG. 9. (Color online) Azimuthal variation of the hydrogen recoil intensity assuming different adsorbate heights. All calculations were performed for 1 keV $Ne^+ \rightarrow W(100)+H(ads)$, assuming a recoil angle of $\theta = 45°$ and a polar angle of $\alpha = 81.5°$. Key azimuths on the surface are indicated on the top axis. The solid line is a spline fit intended to guide the eye between the individual simulations (indicated by the markers).

which would prevent the basic theoretical framework outlined here to this more complex problem.

VIII. ANALYSIS OF PARTIAL- AND LOW-COVERAGE CASES

Based on the discussion presented in the previous section, it is now possible to understand the partial coverage recoil map depicted in Fig. 3(b). As previously mentioned, basic features of this map closely resemble those of the saturation coverage case. However, because the hydrogen surface concentration is significantly lower, the shadowing along the centerline of each of the channels is diminished. This can be calculated directly using the expression for the string potential, V_s, discussed in Sec. VI. The reduced influence of the surface hydrogen causes the features along the ⟨110⟩ directions to be much less distinct. Furthermore, the signal intensity along the ⟨100⟩ directions is also confined to a smaller azimuthal range, partially due to hydrogen deflecting the incident ions to a much lesser extent. From our DFT calculations described in Sec. II, we also noted that the vibrational amplitude perpendicular to the plane containing the W-H-W bond increases as the coverage diminishes. This would contribute to some of the blurring of the hydrogen recoil signals in Fig. 3(b) in comparison to the saturation coverage case.

Finally, consider the case where most of the surface hydrogen on W(100) has been desorbed by heating. Based on the recoil patterns evident in Fig. 3(c), we initially considered the possibility that hydrogen prefers to occupy hollow sites under these conditions. However, such a conclusion would be inconsistent with our DFT calculations that predict these sites have a binding energy 0.4 eV smaller than bridge sites. Such a difference is large enough to ensure the population in fourfold sites would be very small. Furthermore, HREELS measurements did not detect any signs of binding to hollow sites on surfaces. With this in mind, a more plausible explanation may be that hydrogen binds to point defects or other surface features, which, due to the presence of a larger number of nearest neighbors, could be more stable than bridge sites at higher temperatures.

This brings up the question of how one might determine if hydrogen binds to point defects on the surface. One solution may be to prepare a nearly defect-free tungsten surface or one with controlled defect populations (such as steps) and see if the scattering pattern is affected. Hydrogen population of defects might permit conventional medium- and high-energy channeling using the tungsten atoms to shadow the hydrogen.

IX. CONCLUDING REMARKS

Most previous studies that used DRS to determine the hydrogen binding geometry on surfaces have relied on shadow cone analysis. As we have discussed, this restricts the technique to systems where the hydrogen resides close to the surface. In this work we illustrated how a more comprehensive experimental and modeling approach that enables DRS to be applied to systems where the shadow cone method cannot be used. Our experimental maps clearly show that enhanced recoil signals are present along specific crystal azimuths. The preferred adsorption site can be deduced from the maps rather easily by considering different surface channels. This procedure fully captures the recoil behavior over a broad range of incidence angles.

Simulating the scattering and recoil collisions at grazing incidence accurately requires models (e.g., MD) that allow a single incident ion to interact with multiple surface atoms simultaneously. Using these modeling tools, we have shown how the recoil signals vary with adsorbate height as well as the interatomic potential. The combination of these parameters controls ion focusing along surface channels. While an individual hydrogen atom does not have a strong effect on the ion trajectories, our calculations illustrate that the cumulative effect of many hydrogen atoms binding to a surface channel is quite dramatic, and some features in our experiments reveal this effect. The commonly used ZBL potential is much more repulsive at large interatomic separations for the Ne-H and Ne-W interactions than predicted by our DFT or individual pair calculations. Our potentials calculated using the isolated atom electron distributions are more appropriate, since they are more representative of the large impact parameters for these studies of surfaces.

While no single surface analysis can provide a complete description of a given adsorption system, DRS is uniquely sensitive to adsorbed hydrogen and its binding configuration. With some refinement, our analysis indicates that using

the combination of experimental and modeling techniques discussed here it would be feasible to detect adsorbates heights to well within their vibrational envelope. The recoil maps described here are applicable to locating hydrogen on other high-Z metals.

ACKNOWLEDGMENTS

This work was supported through the US Department of Energy, Office of Fusion Energy Sciences as well as the Plasma-Surface Interactions Science Center. In addition, Robert Kolasinski acknowledges support from Sandia's Early Career Laboratory Directed Research and Development program. We express our appreciation to Robert Bastasz, William Wampler, Dean Buchenauer, Rion Causey, Russell Doerner, and Brian Wirth for helpful discussions regarding this work. Sandia is a multiprogram laboratory operated by Sandia Corporation, a Lockheed Martin Company, for the United States Department of Energy's National Nuclear Security Administration under Contract DE-AC04-94AL85000.

*Corresponding author: rkolasi@sandia.gov; Sandia National Laboratories, P.O. Box 969, MS 9161, Livermore, CA 94551, USA.

[1]L. Schlapbach and A. Züttel, Nature **414**, 353 (2001).
[2]C. S. Marchi, B. P. Somerday, X. Tang, and G. H. Schiroky, Int. J. Hydrogen Energy **33**, 889 (2008).
[3]R. A. Causey, J. Nucl. Mater. **300**, 91 (2002).
[4]D. A. King and G. Thomas, Surf. Sci. **92**, 201 (1980).
[5]R. A. Barker and P. J. Estrup, Phys. Rev. Lett. **41**, 1307 (1978).
[6]R. F. Willis, W. Ho, and E. W. Plummer, Surf. Sci. **80**, 593 (1979).
[7]C. Klein, A. Eichler, E. L. D. Hebenstreit, G. Pauer, R. Koller, A. Winkler, M. Schmid, and P. Varga, Phys. Rev. Lett. **90**, 176101 (2003).
[8]R. Bastasz, T. E. Felter, and W. P. Ellis, Phys. Rev. Lett. **63**, 558 (1989).
[9]T. Ito, K. Umezawa, and S. Nakanishi, Appl. Surf. Sci. **147**, 146 (1999).
[10]O. Grizzi, M. Shi, H. Bu, J. W. Rabalais, R. R. Rye, and P. Nordlander, Phys. Rev. Lett. **63**, 1408 (1989).
[11]O. Grizzi, J. E. Gayone, G. R. Gómez, R. G. Pregliasco, and E. A. Sánchez, J. Nucl. Mater. **248**, 428 (1997).
[12]O. S. Oen, Surf. Sci. **131**, L407 (1983).
[13]B. Hird, Can. J. Phys. **69**, 70 (1991).
[14]J. A. White, D. M. Bird, and M. C. Payne, Phys. Rev. B **53**, 1667 (1996).
[15]M. T. Robinson, Phys. Rev. B **40**, 10717 (1989).
[16]A. Schüller, M. Busch, J. Seifert, S. Wethekam, H. Winter, and K. Gartner, Phys. Rev. B **79**, 235425 (2009).
[17]P. J. Estrup and J. Anderson, J. Chem. Phys. **45**, 2254 (1966).
[18]H. Wengelnik, D. Badt, and H. Neddermeyer, Surf. Sci. **307–309**, 619 (1994).
[19]M. R. Barnes and R. F. Willis, Phys. Rev. Lett. **41**, 1729 (1978).
[20]H.-J. Ernst, E. Hulpke, J. P. Toennies, and C. Wöll, Surf. Sci. **262**, 159 (1992).
[21]J. E. Reutt, Y. J. Chabal, and S. B. Christman, Phys. Rev. B **38**, 3112 (1988).
[22]I. Stensgaard, L. C. Feldman, and P. J. Silverman, Phys. Rev. Lett. **42**, 247 (1979).
[23]D. F. Johnson and E. A. Carter, J. Mater. Res. **25**, 315 (2010).
[24]G. Kresse and J. Furthmüller, Comput. Mat. Sci. **6**, 15 (1996).
[25]J. P. Perdew, K. Burke, and M. Ernzerhof, Phys. Rev. Lett. **77**, 3865 (1996).
[26]G. Kresse and D. Joubert, Phys. Rev. B **59**, 1758 (1999).
[27]P. E. Blöchl, Phys. Rev. B **50**, 17953 (1994).
[28]M. Methfessel and A. T. Paxton, Phys. Rev. B **40**, 3616 (1989).
[29]R. Bastasz, J. A. Whaley, T. A. Lograsso, and C. J. Jenks, Phil. Mag. **86**, 855 (2006).
[30]R. D. Kolasinski, J. Whaley, and R. Bastasz, Phys. Rev. B **86**, 075416 (2009).
[31]H. Eleveld and A. van Veen, J. Nucl. Mater. **212–215**, 1421 (1994).
[32]R. Bastasz and J. Whaley, J. Nucl. Mater. **337–339**, 544 (2005).
[33]R. Bastasz, J. W. Medlin, J. A. Whaley, R. Beikler, and E. Taglauer, Surf. Sci. **571**, 31 (2004).
[34]H. Winter, Phys. Rep. **367**, 387 (2002).
[35]D. M. Danailov, D. J. O'Connor, and K. J. Snowdon, Surf. Sci. **347**, 215 (1996).
[36]D. M. Danailov, J. H. Rechtien, and K. J. Snowdon, Surf. Sci. **259**, 359 (1991).
[37]M. A. Karolewski, Nucl. Instrum. Meth. B **230**, 402 (2005).
[38]J. W. Rabalais and J.-N. Chen, J. Chem. Phys. **85**, 3615 (1986).
[39]C. Waldfried, D. N. McIlroy, J. Zhang, P. A. Dowben, G. A. Katrich, and E. W. Plummer, Surf. Sci. **363**, 296 (1996).
[40]C. Lehmann and G. Leibfried, J. Appl. Phys. **34**, 2821 (1963).
[41]J. F. Ziegler, J. P. Biersack, and U. Littmark, *The Stopping and Range of Ions in Solids* (Pergamon Press, New York, 1985).
[42]H. Winter and A. Schüller, Nucl. Instrum. Meth. B **232**, 165 (2005).
[43]M. A. Karolewski, Nucl. Instrum. Meth. B **243**, 43 (2006).
[44]P. T. Wedepohl, Proc. Phys. Soc. **92**, 79 (1967).
[45]E. Clementi and C. Roetti, Atom. Data Nucl. Data **14**, 177 (1974).
[46]R. D. Kolasinski, J. A. Whaley, R. A. Karnesky, C. S. Marchi, and R. Bastasz, Nucl. Instrum. Meth. B **269**, 1229 (2011).